J. Fluid Mech. (1971), *vol.* 45, *part* 4, *pp.* 721–746
Printed in Great Britain

Shock-wave reflexion in a relaxing gas

By RONALD K. HANSON

Department of Aeronautics and Astronautics, Stanford University,
Stanford, California

(Received 16 March 1970)

The transient situation which follows when a plane normal shock wave is reflected (from a coplanar wall) into its own relaxation zone is examined theoretically. Approximate inner and outer solutions for the wall-pressure history are employed to establish the timewise variations in the thermodynamic state of the gas adjacent to the wall. Results for chemically relaxing O_2 and vibrationally relaxing CO_2 are compared with previous numerical solutions based on the method of characteristics, and the agreement is found to be excellent. The approximate technique is simple and requires only a minimum of computing time.

1. Introduction

This paper is concerned with the effects of relaxation on the state of the gas behind a reflected shock wave in a shock tube. In particular, a simple model is described for calculating the transient behaviour of the gas adjacent to a shock-tube end-wall for situations in which relaxation is present both upstream and downstream of the reflected shock wave, i.e. when the primary shock wave reflects into its own relaxation zone. Effects such as shock-wave curvature, side-wall boundary layers, transport processes and heat transfer to the end-wall are neglected throughout.

The theory given here has application to relaxation phenomena in a number of gases, but results are presented only for the cases of chemical relaxation (dissociation and recombination) in oxygen and vibrational relaxation in carbon dioxide. The results of the approximate model can thus be compared with the numerical calculations of Presley & Hanson (1969) for oxygen and of Johannesen, Bird & Zienkiewicz (1967) for carbon dioxide. Both of these earlier studies employed the method of characteristics to obtain rather lengthy numerical solutions for the entire reflected-shock flow field. The intent of the present paper is to provide an approximate solution, valid only in the vicinity of the end-wall, which requires a minimum of computer time.

A primary difficulty of the shock-reflexion process is its unsteady nature. When relaxation phenomena are present the reflected shock wave changes speed during the time required for the upstream and downstream flows to reach equilibrium conditions, and the gas particles which pass through the reflected shock wave during this period experience different thermodynamic histories than those which pass through the later, constant-speed shock wave. Hence these

'early' gas particles ultimately reach different equilibrium states from the state predicted by the usual constant-speed-shock calculations. The spatial region, adjacent to the end-wall, which contains this non-uniform gas can be called an entropy layer; this terminology is consistent with that used to describe the region adjacent to the surface of a wedge in steady supersonic flow of a relaxing gas. Neither the transient nor the steady thermodynamic state of the gas within this entropy layer is known from elementary calculations, with the exception of the pressure, which must eventually take on the value corresponding to a constant-speed reflected shock wave with a uniform equilibrium flow upstream and a stagnated equilibrium flow downstream. Only after the reflected shock attains its final equilibrium speed, and the flow pattern with respect to the reflected shock wave becomes truly steady, does a region of uniform equilibrium gas begin to appear (external to the entropy layer) for which properties can be calculated by usual techniques. Thereafter the reflected-shock region consists of a steadily growing volume of uniform equilibrium gas bounded at one end by the relaxation zone behind the reflected shock wave and at the other by a finite, unchanging entropy layer. The values of the thermodynamic variables within the uniform region are the ones which appear in tables of 'equilibrium reflected-shock properties', and this thermodynamic state will be referred to hereafter as the reference equilibrium state.

In the present work we propose to establish the transient behaviour of the gas immediately adjacent to the end-wall by employing an approximate solution for the wall pressure. It will be shown that a knowledge of the pressure solution, and the appropriate rate law, is sufficient to completely specify the timewise variations in the remaining thermodynamic variables. The key step is the pressure solution, and this is accomplished by taking advantage of the fact that the characteristic relaxation times for the flow behind the incident and reflected shock waves are frequently quite different. Accordingly, separate inner and outer solutions, valid for short and long times respectively, are employed for the wall pressure. A composite solution, obtained by simply combining the two separate solutions, is shown to provide quite accurate results for cases in which the relaxation times are reasonably different.

The overall end-wall pressure history is dominated by the outer solution, and accordingly more attention is given to its development. The inner solution plays only a minor role, but it does provide an important link between the correct initial and final pressure behaviour. This link is necessary for calculating the thermodynamic history of the gas since all the thermodynamic variables must begin with the correct initial values in order to properly satisfy the thermal equation of state.

2. Outer solution for the wall pressure

The behaviour of the wall pressure in the case of a relaxing gas was first discussed by Baganoff (1965). He argued that the effect of relaxation behind the reflected shock wave is to cause a decrease in pressure, while relaxation behind the incident shock wave, on the contrary, causes an increase in wall pressure.

These arguments were subsequently confirmed by the numerical calculations of Johannesen *et al.* (1967) and Presley & Hanson (1969).

Fortunately the time scales of the relaxation processes behind the incident and reflected shock waves are frequently quite different, and in such cases the relaxation effects can, to a remarkable degree of accuracy, be considered separate (Hanson 1968). A simple model for the outer solution, based on this concept of separate relaxation times, can be constructed by supposing that the relaxation zone behind the reflected shock wave is negligibly thick and is absorbed into the

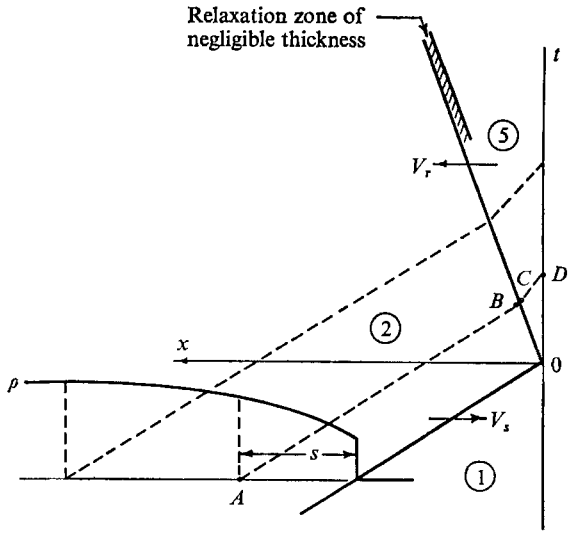

FIGURE 1. x,t diagram of shock-wave reflexion.

viscous structure of the shock front. In fact we assume that the duration of all events associated with the relaxation in the reflected-shock region can be set equal to zero. Such a model is capable of yielding extremely accurate results for long times after reflexion (i.e. times much greater than that corresponding to the passage of a gas particle through the neglected relaxation zone), and this is the technique we propose to pursue here. The results will of course be most valid for situations in which the ratio of the relaxation times is rather large (a precise definition of the relaxation time is not necessary at this stage).

The first step of the proposed outer solution consists of calculating the properties throughout the relaxation zone following the incident shock wave. These computations are usually performed using a computer code based on the conservation relations for one-dimensional flow, the thermal and caloric state relations for the gas in question and the applicable reaction-rate equation. The techniques for solving the incident-shock equations are well documented and need not be discussed here. The important point is that, once the reaction mechanism and the associated rate equation have been specified, the distribution of all properties throughout the relaxation zone can be easily calculated for given values of the shock speed and the initial shock-tube conditions.

Details of the model for the reflexion process are conveniently discussed using

the x, t diagram of figure 1, where x is the distance from the shock-tube end-wall and t is the time after initial reflexion; s is the distance behind the incident shock wave. The incident shock wave travels toward the end-wall at a constant speed V_s and the reflected shock wave is assumed (consistently with the assumptions of an outer solution) to reflect with a constant speed V_r, taken here to be the final, equilibrium value of shock speed corresponding to equilibrium (chemical or vibrational) upstream and downstream of the reflected shock wave, i.e. $(V_r)_{E2-E5}$. A qualitative profile of the density (ρ) distribution throughout the incident-shock relaxation zone is also shown. This profile would appear as if it were travelling across the x, t plane attached to the incident shock wave.

The wall pressure at time zero is given by a calculation assuming frozen conditions in region 2 and local equilibrium in region 5, i.e. P_{F2-E5}. Thereafter the pressure rises asymptotically to the final, equilibrium value, P_{E2-E5}, based on equilibrium conditions in region 2 and region 5. Values for the pressure at intermediate times are computed by a simple mapping technique which transforms the spatial variations in density throughout region 2 into temporal variations in pressure on the end wall. Details of this mapping technique, together with justifications for its use, form the subject of the following paragraphs.

The first step in the mapping process consists of projecting (unchanged) the known properties at point A across the x, t plane to form the upstream boundary conditions for the reflected shock wave at point B. The state of the gas at point C immediately behind the shock front is then known from standard shock-jump relations since the gas is assumed to be in local equilibrium. The pressure at point C can be transferred across region 5 along a characteristic terminating at point D. Since the gas is assumed to be in local equilibrium, the pressure is unchanged along this characteristic save for small variations accounting for any change in particle velocity. The characteristics may be considered straight for all practical purposes as only small variations in temperature and particle velocity occur in region 5 for this problem. For convenience all of the right-running characteristics are taken to have a slope given by the equilibrium speed of sound evaluated at the reference equilibrium state, i.e. $dx/dt = -(a_e)_{E2-E5}$.

The complete wall-pressure history can be constructed from a number of these transformations, each originating at a different position behind the incident shock wave. Since the relaxation profiles in region 2 are uniquely determined by the rate law specified, a unique relation also exists between the rate law chosen and the computed wall-pressure history.

In the real case the reflected shock wave moves away from the end-wall with a speed which changes with time. As the gas begins to relax in region 5 the shock speed rapidly decays from its initial, frozen value, $(V_r)_{F2-F5}$, to a value approaching $(V_r)_{F2-E5}$. Since the time required for this change to take place is comparable to the relaxation time in region 5, we may assume, for the purpose of constructing an outer solution, that the change occurs in zero time. Then, in a time of the order of the laboratory relaxation time in region 2, i.e. τ_{2L}, the shock speed increases to a final value $(V_r)_{E2-E5}$. Fortunately there is little difference between the values of $(V_r)_{F2-E5}$ and $(V_r)_{E2-E5}$, and considerable simplification can be realized by choosing a constant-speed shock trajectory with a slope of $(V_r)_{E2-E5}$.

In fact, with this approximation, and one other regarding the gas-state calculations at point C, the pressure at point D can be written explicitly in terms of the density at point A, as shown below.

The pressure at point C is given by standard shock-jump relations as

$$P_C = P_B + \rho_B (U_B + V_r)^2 (1 - \rho_B/\rho_C), \tag{1}$$

where, from the conservation of mass,

$$\rho_B/\rho_C = (V_r + U_C)/(V_r + U_B). \tag{2}$$

In these relations U_B is the speed of the gas toward the end-wall at point B,

$$U_B = V_s(1 - \rho_1/\rho_B), \tag{3}$$

and U_C is the speed of the gas toward the wall at point C. Numerous calculations have shown that $U_C \ll V_r$, so the ratio ρ_B/ρ_C is well approximated by

$$\rho_B/\rho_C = V_r/(V_r + U_B). \tag{4}$$

This last result is physically plausible since one would expect the flow to be nearly stagnant everywhere in region 5 except within the relaxation zone.

From incident-shock relations, one can write

$$P_B = P_1 + \rho_1 V_s^2 (1 - 1/\eta_B), \tag{5}$$

where the symbol η_B is used to denote the local value for the density ratio across the incident shock wave, ρ_B/ρ_1. Upon substitution of (3), (4) and (5), (1) becomes simply

$$P_C = P_1 + \rho_1 V_s^2 (\eta_B - 1)(1 + V_r/V_s), \tag{6}$$

where $(1 + V_r/V_s)$ is a constant because of the assumption imposed on the reflected shock speed. Furthermore, $P_C/P_1 \gg 1$ for shock waves strong enough to produce relaxation, so that one has the simple result

$$P_C/P_{E2-E5} = P_C/P_5^* = (\eta_B - 1)/(\eta_{E2} - 1). \tag{7}$$

An asterisk will be used hereafter to denote the reference equilibrium conditions in region 5 (the state previously denoted by $E2$–$E5$).

Since the velocity U_C was taken as zero, P_D can be set equal to P_C, and the pressure on the end-wall at point D can be written explicitly in terms of the density at point A, i.e.

$$P_D/P_5^* = (\eta_A - 1)/(\eta_{E2} - 1). \tag{8}$$

This particularly simple result is quite reasonable if one remembers that the static pressure in region 5 is essentially proportional to the upstream dynamic pressure, and the dynamic pressure involved varies almost linearly with the density alone (since the relative velocity of the gas and the reflected shock wave is nearly constant). The correct asymptotic behaviour of this last expression is obvious.

Since the time at point D can be written directly in terms of the distance s at point A,

$$t_D = (s_A/V_s)(1 + V_r/a_e^*)/(1 + V_r/V_s), \tag{9}$$

where a_e^* is the equilibrium speed of sound evaluated at the reference equilibrium state, the outer solution for the wall pressure is now completely specified once the density distribution in region 2 is known.

It is worth noting that the equilibrium speed of sound, rather then the frozen speed of sound, has been used for the slope of the characteristics in order to be consistent with the assumption of local equilibrium throughout region 5. For a discussion of the equilibrium speed of sound in a relaxing gas see, for example, Vincenti & Kruger (1965).

We are now in a position to demonstrate the accuracy of the outer solution technique by comparing results with numerical calculations based on the method of characteristics. Figures 2 and 3 present such comparisons for two different shock waves in chemically relaxing oxygen. The characteristics calculations were performed at NASA Ames Research Center (Presley & Hanson) and have been labelled 'Ames solution'. The chemical reaction considered was

$$O_2 + M \underset{k_r}{\overset{k_d}{\rightleftharpoons}} 2O + M \tag{10}$$

where k_d and k_r are the dissociation and recombination rates respectively, and M represents a general collision partner, in this case either an atom or molecule of oxygen. The rate law was specified by

$$\rho D\alpha/Dt = W[M]\, k_r\{K[O_2] - [O]^2\}, \tag{11}$$

where W is the molecular weight of O_2, α is the mass fraction of the O-atom species, K is the usual equilibrium constant and the square brackets are used to denote species concentrations (in moles/cm^3). This form of the rate equation includes the common assumption that the ratio of the dissociation and recombination rates is equal to the equilibrium constant evaluated at the local translational temperature. Numerical values for the recombination rate were calculated from

$$k_r = 7{\cdot}3 \times 10^{21} T^{-2}\ [\mathrm{cm}^6/(\mathrm{mole}^2\,\mathrm{sec})], \tag{12}$$

while values for the equilibrium constant were computed from statistical mechanics on the assumption that the gas remains electronically unexcited (see Presley & Hanson).

The agreement between the outer solution and the Ames solution is remarkably good in figure 2 and figure 3. In fact, the outer solutions deviate less than 2 % from the characteristics solutions except during the brief initial period of time wherein the relaxation in region 5 is important. For such short times an inner solution becomes useful. The agreement shown in figure 2, the case of a moderately strong shock wave ($\alpha_{2E} \simeq 0{\cdot}1$), begins to deteriorate slightly for large time, but the disagreement is a result of difficulty with the Ames solution rather than error in the outer solution. This difficulty, involving small oscillations in the values of pressure and particle velocity throughout the characteristics network, was the primary motive for ending the calculations at a time of 35 μsec. These oscillations were a function of the network mesh size and hence could only be reduced at the expense of increasing the computing time (which already amounted to more than 4 h). The characteristics solution in figure 3, the case of a stronger shock wave

($\alpha_{2E} \simeq 0{\cdot}25$), was terminated for the same reason although the disagreement with the outer solution at large time is less pronounced.

We can demonstrate the accuracy of the outer solution for a vibrationally relaxing gas by utilizing the results presented by Johannesen *et al.* (1967) for CO_2. Johannesen's group treated the shock-reflexion problem numerically by making use of the characteristic equations for one-dimensional unsteady flow with

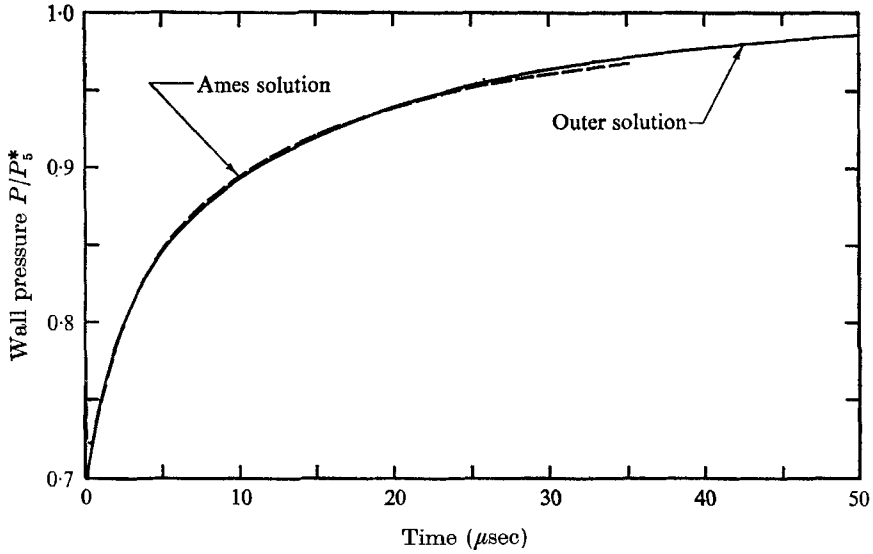

FIGURE 2. Comparison of long-time wall-pressure histories in chemically relaxing O_2; $V_s = 3{\cdot}05$ km/sec, $T_1 = 294$ °K, $P_1 = 2$ torr and $k_r = 7{\cdot}3 \times 10^{21} T^{-2}$ [cm^6/(mole^2 sec)].

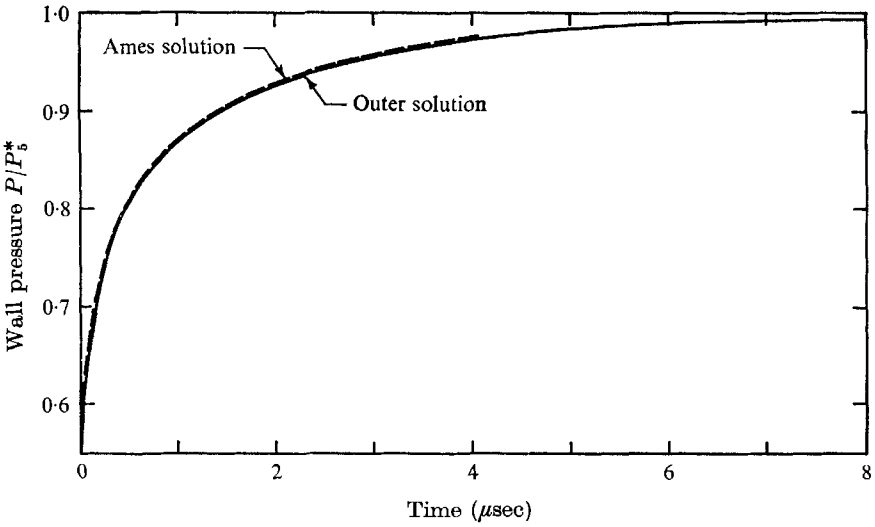

FIGURE 3. Comparison of long-time wall-pressure histories in chemically relaxing O_2: $V_s = 3{\cdot}96$ km/sec, $T_1 = 294$ °K, $P_1 = 2$ torr and $k_r = 7{\cdot}3 \times 10^{21} T^{-2}$ [cm^6/(mole^2 sec)].

heat transfer. The heat-transfer term was set equal to the rate of vibrational excitation according to the Bethe–Teller rate law,

$$D\sigma/Dt = (\bar{\sigma} - \sigma)/\tau, \tag{13}$$

where σ is the vibrational energy and $\bar{\sigma}$ its local equilibrium value. The parameter τ, the relaxation time, was specified by Johannesen on the basis of a curve fit to previous experimental data (Johannesen, Zienkiewicz, Blythe & Gerrard 1962), i.e. in their notation,

$$P\tau \text{ (atm sec)} = (T/273)/\Phi_\theta \hat{\Phi}(T), \tag{14}$$

where T is the absolute temperature, $\Phi_\theta = 2{\cdot}5 \times 10^6$ (sec Amagat)$^{-1}$, and

$$\hat{\Phi}(T) = (T/959)\exp[2{\cdot}02 - 2{\cdot}48(T/959)^{-\frac{1}{3}}][1 - \exp(-959/T)]^{-1}. \tag{15}$$

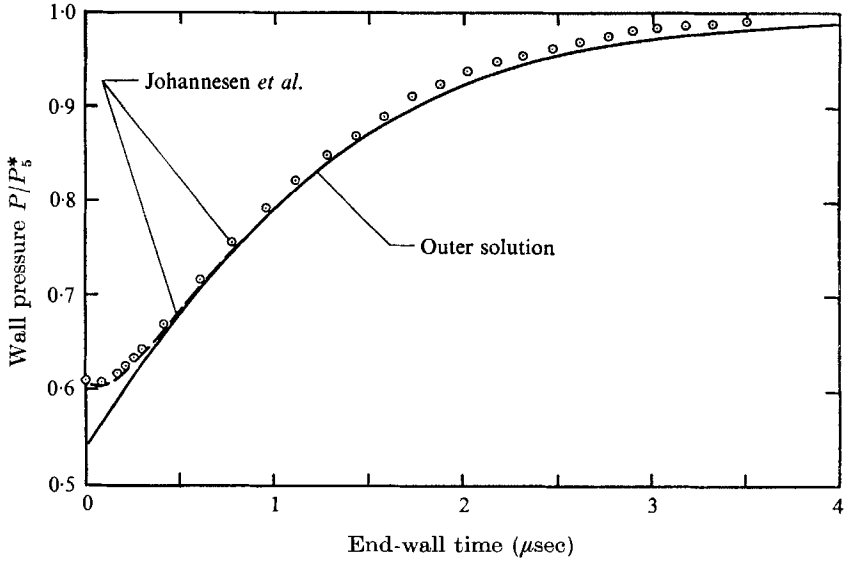

FIGURE 4. Comparison of long-time wall-pressure histories for vibrationally relaxing CO_2: $V_s = 1{\cdot}62$ km/sec, $T_1 = 300$ °K and $P_1 = 1$ torr. – –, small steps; ⊙, large steps.

It was necessary to read the above value for Φ_θ (the relaxation frequency at 959 °K) from figure 5 of Johannesen's (1962) earlier paper since he did not specify the particular value used in his reflected-shock calculations. There is, therefore, a chance that the value of Φ_θ used in the outer-solution calculations differs slightly from the value employed by Johannesen.

Figure 4 provides a comparison between the wall-pressure history computed with the outer solution and the characteristics results presented by Johannesen *et al.* (1967). Note that the characteristics computations were carried out for two different step sizes (the small steps, one-fifth the size of the large steps, yield a solution about 1 % lower than the large-step solution). The agreement between the outer solution and the small-step computation is quite good, except for very small values of time, and it is tempting to suggest that calculations based on a still smaller step size would provide even better agreement.

The deviation between the small- and large-step results for short times during which both computations are available (the small-step solution was apparently terminated at about 0·8 μsec) implies that an accumulative error is present in the large-step solution. Hence the large-step characteristics solution cannot be applied as a rigorous standard of comparison for the outer solution even for large values of time. However, the guaranteed asymptotic behaviour of the outer solution, and the excellent agreement found with the small-step solution at short times, provide strong support for applying the outer solution with confidence for all but very short times. In fact, apart from the initial period immediately following reflexion, the outer solution is almost certainly more accurate than the present characteristics results.

With the accuracy of the outer solution established for the circumstances described above, it is appropriate to comment on the applicability of the outer solution to other gases and test conditions. We recall that the basic hypothesis upon which the technique rests is that the relaxation time in region 2 should be much greater than the corresponding relaxation time in region 5. A simple comparison of these relaxation times should therefore enable one to distinguish situations which can be successfully treated with this approach.

We examine first the somewhat simpler case of vibrational relaxation. The presence of simultaneous chemical reactions is not considered. The characteristic relaxation time for vibrational relaxation can generally be expressed in the form

$$P\tau = A \exp(BT^{-\frac{1}{3}}), \tag{16}$$

where A and B are positive constants which depend on the physical character of the gas in question. The ratio of the relaxation times in regions 2 and 5 is therefore (in laboratory time)

$$\tau_{2L}/\tau_{5L} = (P_5/P_2)(P\tau)_2/\eta(P\tau)_5, \tag{17}$$

where we have assumed that the laboratory value for the relaxation time in region 5 is essentially the same as the particle time, and the laboratory relaxation time in region 2 is approximately equal to the particle time divided by the incident-shock density ratio, η.

This last relation can be simplified considerably if we make use of the reasonable approximations that $T_5 \simeq 2T_2$ and $P_5 \simeq \eta P_2$. The result of these substitutions is

$$\tau_{2L}/\tau_{5L} \simeq \exp(0{\cdot}2BT_2^{-\frac{1}{3}}). \tag{18}$$

The outer solution should therefore be most accurate for gases which have large values of B. Gases such as N_2, CO and O_2, for example, have larger values of B than CO_2. (For information regarding the values of B in several common gases, see Millikan & White 1963*a*.) The ratio of the relaxation times also becomes more favourable at lower temperatures (i.e slower shock speeds) in a given gas.

In order to provide specific numbers for the CO_2 case shown in figure 4, we must make use of the particular rate expression (see (14) and (15)) employed in those calculations, since it is not of the form specified above in (16). The result of the computation, based on the frozen conditions in regions 2 and 5, is

$$\tau_{2L}/\tau_{5L} \simeq 4. \tag{19}$$

This ratio is not nearly as large as one might have expected on the basis of the good agreement shown in figure 4. The reason for this apparent discrepancy is due, in large part, to not having included in the analysis the relative influence of the relaxation in regions 2 and 5. That is, while the effect of relaxation in region 5 is to cause a decrease in wall pressure (for a gas which remains frozen in region 2), the subsequent (or simultaneous) effect of relaxation in region 2 is to cause an increase in pressure some 3 to 6 times as large. A representative calculation of the 'effective' relaxation-time ratio should include this factor. The effective ratio provides a more meaningful criterion for the potential accuracy of the outer solution.

For the case of shock-wave reflexion in CO_2 under consideration here, the 'pressure-influence' factor is about 6 so that the effective ratio of the relaxation times is about 24. The magnitude of this number is consistent with the accuracy exhibited by the outer solution in figure 4.

To illustrate the improvement in the outer solution which might be expected with a more favourable gas, consider the relaxation-time ratio for a Mach 8 shock wave in N_2. A value of B equal to 235 is given by Millikan & White (1963*b*) and a reasonable value for T_2 is 3750 °K. Substitution of these numbers into (18) yields a relaxation-time ratio of 20. The appropriate pressure-influence factor is about 4, so the effective relaxation-time ratio is about 80. The outer solution should provide extremely accurate results for such a gas, but unfortunately no exact solutions for wall-pressure histories in N_2 are available for quantitative comparison.

A similar calculation for the relaxation times in a chemically relaxing gas can also be made. Using the rate law in (11), for example, a characteristic relaxation time based on the frozen conditions in region 5 is

$$\tau_{5L} \simeq (W/\rho k_d)_{5F}. \tag{20}$$

The appropriate laboratory relaxation time in region 2 is, accordingly,

$$\tau_{2L} \simeq (W/\eta\rho k_d)_{2F}. \tag{21}$$

If we assume that the dissociation rate can be expressed in the form

$$k_d = AT^{-B}\exp(-\theta_d/T), \tag{22}$$

where θ_d is the characteristic temperature for dissociation, and introduce the further approximations that $B \simeq 2$, $T_{5F} \simeq 2T_{2F}$ and $\rho_{5F} \simeq 4\rho_{2F}$, we obtain the simple result that

$$\tau_{2L}/\tau_{5L} \simeq (1/\eta_F)\exp(\theta_d/T_{5F}). \tag{23}$$

This analysis is implicitly restricted to shock waves which are strong enough to cause significant dissociation in region 2, but too weak to cause significant ionization in region 5. For O_2 the corresponding shock-strength range is about Mach 7 to 14, so the frozen temperature is bounded approximately by

$$3{\cdot}5 \lesssim \theta_d/T_{5F} \lesssim 12. \tag{24}$$

(These temperatures were computed on the assumption that all the internal energy modes were equilibrated at the local translational temperature.) The

results of (24) are typical of other diatomic gases as well, and it is obvious that, except for very strong shock waves, the relaxation-time ratio expressed in (23) can be enormous. Bearing in mind further that these figures do not include the pressure-influence factor discussed above, the excellent agreement found in figures 2 and 3 is clearly justified.

The simplicity and accuracy of the outer solution, for cases involving either chemical or vibrational relaxation, suggest the feasibility of using end-wall pressure measurements to obtain relaxation-rate information. Indeed, the ability to perform such experiments and the lack of a satisfactory theory for reducing the data (with a reasonable expenditure of computer time) were primary motivations for the present theoretical effort. For an application of this technique to a determination of the vibrational relaxation rate in CO, see Hanson (1970).

3. Inner solution for the wall pressure

The results of the previous section have verified the utility of the outer solution as a simple and accurate means of calculating end-wall pressure histories in a relaxing gas, if the relaxation-time ratio is reasonably large. The outer solution predicts the incorrect short-time behaviour, however, and with the objective of improving this situation we propose to pursue a simple inner solution based on an initial-slope calculation.

The theory for the initial rate-of-change of wall pressure in a vibrationally relaxing gas has already been presented by Johannesen *et al.* (1967), and their results can be employed directly here. For the case of a chemically relaxing gas, however, we prefer to use a slightly different approach which relies rather more on physical intuition. Since this new approach provides an alternative to Johannesen's technique (which could also be extended to cases involving chemical relaxation), it is worthwhile to use this opportunity to illustrate the method and to demonstrate the accuracy which can be expected. The theory for the initial slope in a chemically relaxing gas follows directly below.

Although the inner solution is to be applied only during times of the order of that required for the gas to relax in region 5, a period during which one might expect this relaxation to dominate the wall-pressure history, the effects of relaxation in region 2 can also exert a strong influence and hence must be included in the analysis. For simplicity, however, we assume that the chemical relaxation in regions 2 and 5 produces independent changes in the wall pressure. The initial slope of the wall pressure will thus be composed of two separate contributions.

We begin by writing the pressure as a function of the density in regions 2 and 5, i.e.

$$P_5 = P_1[1+\gamma M_s^2(\eta-1)(\xi-1)/(\xi-\eta)] \simeq P_1\gamma M_s^2(\eta-1)(\xi-1)/(\xi-\eta), \qquad (25)$$

where $\eta = \rho_2/\rho_1$ and $\xi = \rho_5/\rho_1$, and γ is the specific-heat ratio for the translational and rotational degrees of freedom only. The Mach number, M_s, is defined by

$$M_s = V_s/(\gamma RT_1)^{\frac{1}{2}}. \qquad (26)$$

Equation (25) is strictly correct only for a constant-speed reflected shock wave with uniform conditions upstream and stagnated flow downstream. For the purpose of an initial-slope calculation, however, we can assume that the speed of the reflected shock wave adjusts to upstream changes in η and end-wall changes in ξ such that (25) remains valid.

Consider first the effects of relaxation in region 5 (i.e. changes in ξ). The initial slope of the wall pressure is related to the initial slope of the density ratio by

$$\left(\frac{\partial P_5}{\partial t}\right)_{\substack{x=0\\t=0}} = \left(\frac{\partial P_5}{\partial \xi}\right)_{\eta} \left(\frac{\partial \xi}{\partial t}\right)_{\substack{x=0\\t=0}} = -P_1 \gamma M_s^2 \left[\left(\frac{\eta-1}{\xi-\eta}\right)^2 \frac{\partial \xi}{\partial t}\right]_{\substack{x=0\\t=0}}. \tag{27}$$

Since it is our expressed intent to calculate only the initial rate-of-change of pressure, all properties will necessarily be evaluated using the frozen shock conditions, and the subscripts for x and t equal to zero may be dropped. Because the gas particles undergo adiabatic changes (heat transfer to the wall has been neglected throughout this work), the change in wall pressure may also be written as

$$\partial P_5/\partial t = \rho_5(\partial h_5/\partial t). \tag{28}$$

It is necessary now to be more specific about the caloric and thermal equations of state, and we therefore restrict our attention to a homonuclear diatomic gas such as O_2. If electronic excitation is neglected, the enthalpy per unit mass is simply

$$h = (1-\alpha)\left[\tfrac{7}{2}RT + \sigma\right] + \alpha(5RT + D), \tag{29}$$

where R is the gas constant, D is the dissociation energy and σ is the vibrational energy, all per unit mass of the molecular species. Assuming that the vibrational energy mode is equilibrated with the translational temperature, we know that

$$\sigma = \bar{\sigma}(T) = R\Theta_v/[\exp(\Theta_v/T) - 1], \tag{30}$$

where Θ_v is the characteristic vibrational temperature. The thermal equation of state for the dissociating gas is simply

$$P = \rho RT(1+\alpha). \tag{31}$$

A manipulation of the differential forms of (29), (30) and (31), together with (28), permits one to write the initial slope of ξ as

$$\partial \xi/\partial t \simeq \xi[(7/9P_5)(\partial P_5/\partial t) + \tfrac{2}{9}\Psi(T_5)(\partial \alpha/\partial t)_5], \tag{32}$$

where

$$\Psi(T) = (\Theta_d/T - 3 - \bar{\sigma}/RT).$$

Equation (32) includes the approximation that $\partial\bar{\sigma}/\partial T \simeq R$, which is quite acceptable for the temperatures of interest in this application ($T_5 \gtrsim 2\Theta_v$). If one now combines (27) and (32), and makes use of (25) (in its approximate form) to simplify the result, the initial slope of the wall pressure owing to chemical relaxation in region 5 may be written as

$$\left(\frac{1}{P_1}\right)\frac{\partial P_5}{\partial t} \simeq -\tfrac{2}{9}\gamma M_s^2 \xi \left(\frac{\eta-1}{\xi-\eta}\right)^2 \left[1 + \frac{7}{9}\frac{\xi}{\xi-\eta}\frac{\eta-1}{\xi-1}\right]^{-1} \Psi(T_5)\left(\frac{\partial \alpha}{\partial t}\right)_5, \tag{33}$$

where

$$(\partial \alpha/\partial t)_5 = \rho_5 k_d(T_5)/W = \xi P_1 k_d(T_5)/WRT_1.$$

We turn now to a consideration of the role played by the relaxation in region 2 (i.e. changes in η). The sensitivity of the wall pressure to η is stated by (25), while the rate at which changes in wall pressure occur can be linked to the spatial gradient in η through (9). The result for the initial slope of the wall pressure is, accordingly,

$$\frac{\partial P_5}{\partial t} = \left(\frac{\partial P_5}{\partial \eta}\right)_\xi \left[\frac{1+V_r/V_s}{1+V_r/a_f}\right] V_s(\partial\eta/\partial s)$$

$$= P_1 \gamma M_s^2 \left(\frac{\xi-1}{\xi-\eta}\right)^2 \left[\frac{1+V_r/V_s}{1+V_r/a_f}\right] \eta(D\eta/Dt). \tag{34}$$

In this instance V_r refers to the frozen value of the reflected shock speed, $(V_r)_{F2-F5}$, and it is appropriate to use the frozen sound speed evaluated at the conditions present immediately after shock reflexion, $(a_f)_{F2-F5}$.

Variations in η can be related to changes in α through the incident-shock conservation relations and the caloric and thermal equations of state. The result is

$$D\eta/Dt \simeq \tfrac{2}{9}\eta[1-\tfrac{7}{9}(\eta-1)^{-1}]^{-1}\Psi(T_2)(D\alpha/Dt)_2, \tag{35}$$

where

$$(D\alpha/Dt)_2 = \eta P_1 k_d(T_2)/WRT_1.$$

(Details of this derivation are provided in the appendix.) Substitution of (35) into (34) permits one to write the initial slope in wall pressure owing to chemical relaxation in region 2 as

$$\frac{1}{P_1}\frac{\partial P_5}{\partial t} = \tfrac{2}{9}\gamma M_s^2 \eta^2 \left(\frac{\xi-1}{\xi-\eta}\right)^2 [1-\tfrac{7}{9}(\eta-1)^{-1}]^{-1} \left[\frac{1+V_r/V_s}{1+V_r/a_f}\right] \Psi(T_2)(D\alpha/Dt)_2. \tag{36}$$

The combined solution for the initial slope of the wall pressure is given by the sum of (33) and (36). Note that the effect of relaxation in region 2 always provides a positive contribution to the initial slope since all the terms on the right-hand side of (36) are positive (for the full range of conditions of interest here). On the contrary, the effect of relaxation in region 5 may bring about either a negative or a positive contribution to the initial slope depending on the sign of $\Psi(T_5)$. The parameter Ψ changes sign at a shock strength of about Mach 12 in O_2 ($T_5 \simeq \frac{1}{4}\Theta_d \simeq 15{,}000\,^\circ\mathrm{K}$), which is well below the shock strength needed to completely dissociate the gas in region 5.

A plot of the initial slope *versus* shock speed in chemically relaxing O_2 is shown in figure 5. Since the rate-of-change of α in region 2 and region 5 is proportional to the initial pressure, it is convenient to plot a single curve, valid for all pressures, for $(\partial P_5/\partial t)/P_1^2$. With the aim of providing a realistic estimate for the initial slope, the calculations were carried out using the dissociation-rate values suggested by Wray (1962), namely

$$k_d(T) = 2{\cdot}25 \times 10^{12} T^{\frac{1}{2}} (\Theta_d/T)^{1{\cdot}5} \exp(-\Theta_d/T)\,[\mathrm{cm}^3/(\mathrm{mole\ sec})]. \tag{37}$$

For weak shock waves, and hence rather low temperatures, the relaxation in region 5 is dominant, thereby producing a negative initial slope of small magnitude. As the shock strength increases, the reaction rate in region 5 grows

rapidly, hence causing a larger rate-of-decay in the pressure. For yet stronger shock waves, relaxation in region 2 beomes important, and finally, owing to this influence, the initial slope turns positive. For shock strengths above Mach 12,

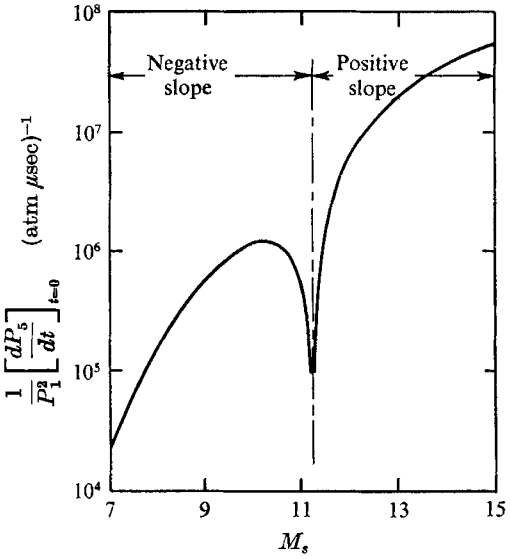

FIGURE 5. Initial rate-of-change of wall pressure in chemically relaxing O_2: $T_1 = 300\,^\circ$K, $\gamma = 1{\cdot}4$ and $k_d = 2{\cdot}25 \times 10^{12} T^{\frac{1}{2}}(\theta_d/T)^{1{\cdot}5} \exp(-\theta_d/T)$ [cm^3/(mole sec)].

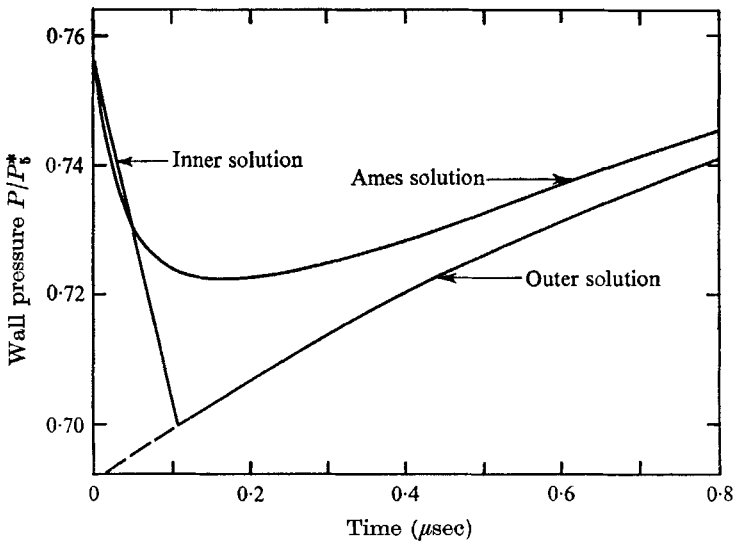

FIGURE 6. Comparison of short-time wall-pressure histories in chemically relaxing O_2: $V_s = 3{\cdot}05$ km/sec, $T_1 = 294\,^\circ$K, $P_1 = 2$ torr and $k_r = 7{\cdot}3 \times 10^{21} T^{-2}$ [cm^6/(mole^2 sec)].

the effect of relaxation in region 5 also yields a positive contribution to the initial slope. The magnitude of the initial slope continues to rise with increasing shock strength owing to the growing values for the dissociation rates. Similar results would be exhibited by other gases.

The accuracy of the initial-slope calculation for a chemically relaxing gas is demonstrated in figure 6 for the same case of shock-wave reflexion shown earlier in figure 2. Comparison is again made with the numerical solution based on the method of characteristics, and the agreement is good. The inner solution based on this initial-slope calculation consists of a simple linear decay from the initial value of wall pressure, P_{F2-F5}/P_5^*. A composite solution is obtained by simply patching the inner and outer solutions together at their intersection.

While further improvement in this inner solution is obviously possible (e.g. by employing an exponential decay rate), such refinements are not necessary for our present purposes. Our major objective is to establish a pressure history

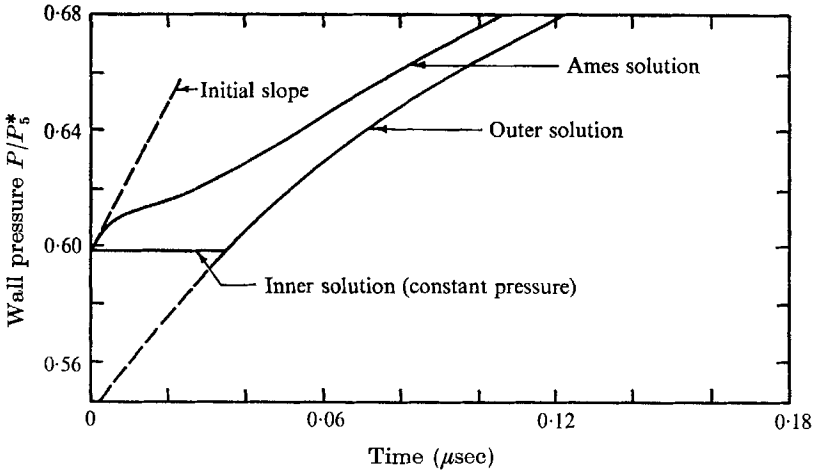

FIGURE 7. Comparison of short-time wall-pressure histories in chemically relaxing O_2: $V_s = 3{\cdot}96$ km/sec, $T_1 = 294$ °K, $P_1 = 2$ torr and $k_r = 7{\cdot}3 \times 10^{21} T^{-2}$ [cm^6/(mole^2 sec)].

which can be successfully employed in the calculation of other end-wall thermodynamic properties. Details of the initial pressure history are therefore not critical since the variations in the thermodynamic properties during this time period are controlled primarily by the rate at which the dissociation reaction proceeds. It is important, however, that all the thermodynamic properties, including the pressure, begin with their correct initial (frozen) values, and this objective is achieved with the present crude model. Details of the pressure history are important for large values of time, of course, since the gas then remains essentially in local chemical equilibrium and changes its thermodynamic state only because of the work done on the gas as it is compressed.

The initial-slope result for a stronger shock wave in O_2 is shown in figure 7 (see figure 3 for the corresponding outer solution). Again the agreement with the initial slope of the Ames solution is good. The unusual structure of the Ames results, which begin with a steep initial slope followed by a decrease in slope and then another increase, can be understood from (33). In this case $\Psi(T_5)$ is initially negative so that the effect of relaxation in region 5 is to help raise the pressure from the frozen value rather than to decrease it. The first decrease in the slope

of the Ames solution occurs because of the rapid decrease in temperature which reverts the sign of $\Psi(T_5)$ back to its usual positive condition. As the temperature in region 5 decreases further, the relaxation in region 2 becomes dominant, thus causing a new increase in the slope. For shock conditions such as these, an inner solution based on the initial slope would never intersect the outer solution, and a composite solution must be formed by a different technique. For our purposes it is sufficient to assume that the pressure remains constant until the outer solution reaches the frozen-pressure level.

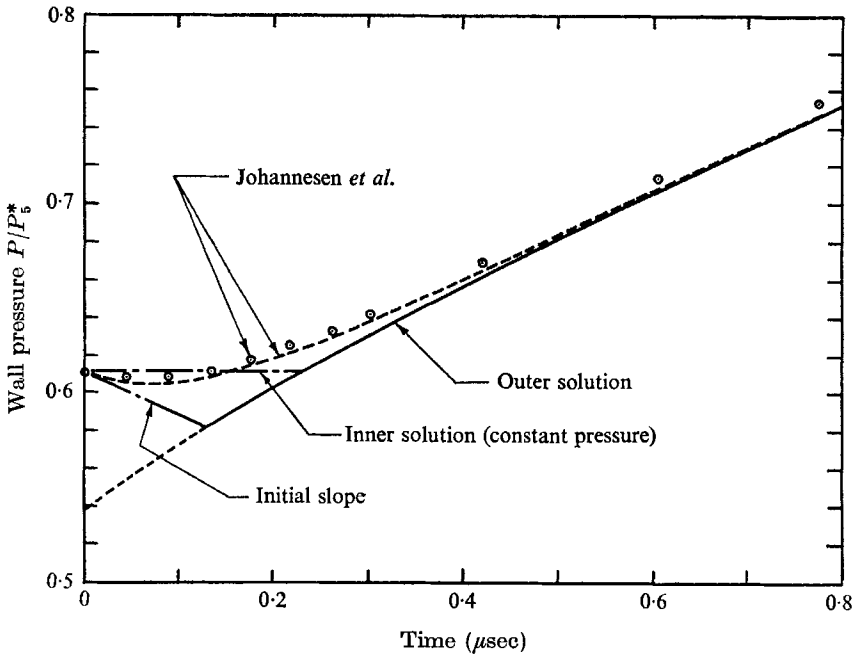

FIGURE 8. Comparison of short-time wall-pressure histories in vibrationally relaxing CO_2: $V_s = 1{\cdot}62$ km/sec, $T_1 = 300$ °K and $P_1 = 1$ torr. – –, small steps; O, large steps.

Information necessary to compute the initial slope of the wall pressure in vibrationally relaxing CO_2 appears in (A 11) and figure A 2 of Johannesen *et al.* (1967). The important observation to be drawn from those results is that the initial slope is always negative, except for shock waves of strength less than Mach 2. Short-time results for the CO_2 case previously discussed here are shown in figure 8 (see figure 4 for the outer solution). The agreement between the initial slope and the characteristics calculation is good at very short times but rapidly degenerates. In such cases it is more practical to select a constant-pressure inner solution, as shown in figure 8, although the particular inner solution chosen has only a small effect on the computed histories of the other thermodynamic properties. The decision whether to employ the initial-slope or constant-pressure inner solution can be made from a simple comparison of the magnitudes of the initial slope and the initial rate-of-increase in pressure presented by the outer solution. For chemical relaxation the separation in the relaxation times is

generally so large, except for very strong shock waves, that an inner solution based on the initial slope is useful. For vibrational relaxation, however, the relaxation times are likely to be much less separate, and a constant-pressure assumption may often be preferable.

4. Solution for the time-varying thermodynamic state

The previous sections have described an approximate technique for predicting the end-wall pressure history. It is shown here that once a pressure solution has been formulated the time evolution of other end-wall thermodynamic properties can readily be found. The validity of this approach is again confirmed by comparison with results based on the method of characteristics.

Variations in the thermodynamic state are calculated by applying the energy equation for one-dimensional adiabatic flow,

$$DP/Dt - \rho\, Dh/Dt = 0, \tag{38}$$

to the element of gas located adjacent to the end-wall. For this particular gas element the velocity is identically zero and the energy equation reduces to (28). The thermodynamic history of the gas follows directly from simultaneous numerical integration of (28) and the appropriate rate equation.

Consider again the case of chemically relaxing O_2. The initial thermodynamic state is known from standard reflected-shock calculations assuming frozen chemistry and instantaneous equilibration of the internal energy modes with the translational temperature. Using the known solution for pressure, one can compute the value of h and α at time $t = \delta t$ by integrating (28) and (11) respectively; e.g.

$$\alpha_{t=\delta t} = \alpha_{t=0} + (D\alpha/Dt)_{t=0}\,\delta t = (D\alpha/Dt)_{t=0}\,\delta t. \tag{39}$$

Knowledge of h, P and α at $t = \delta t$ is sufficient to fix the value of T from the caloric equation of state, (29), and the value of ρ from the thermal equation of state, (31). These new values for the thermodynamic variables can be used to establish a new numerical value for the rate-of-change of α. The calculations continue until the final pressure is reached; at that time a steady equilibrium state will have been attained.

Figures 9 and 10 provide comparisons of end-wall histories in O_2 calculated with the present model and with the Ames program. The agreement is quite remarkable, especially when one considers the difference in computing time (a few hours per case for the Ames program as against less than a minute for the present model). It is also important to note that the Ames results stop short of steady-state conditions so that values are not obtained for the final end-wall state; the present model obtains this information quite readily. Since both calculational techniques utilize integration procedures, some numerical error is introduced by a finite step-size. This error was investigated in the present study, and a step-size was selected such that the error can be neglected on the scale used for plotting figures 9 and 10.

As noted previously, the present gas model does not account for electronic excitation. Since oxygen has some relatively low-lying atomic and molecular

electronic-energy levels, these would have to be considered in a more realistic model. However, the effect of their inclusion on the present results would only be to change slightly the initial and final values of all properties; the shape and time scale of the profiles would not be significantly affected.

One immediate observation which can be made from these results is that the assumption of two separate time scales is valid for the end-wall properties. For

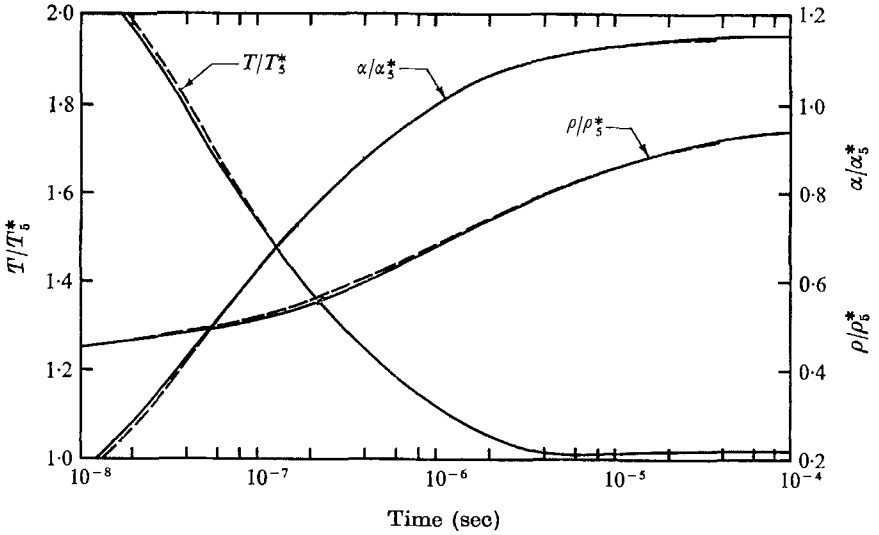

FIGURE 9. Comparison of solutions for end-wall thermodynamic properties in chemically relaxing O_2: $V_s = 3{\cdot}05$ km/sec, $T_1 = 294$ °K, $P_1 = 2$ torr and $k_r = 7{\cdot}3 \times 10^{21} T^{-2}$ (cm^6/(mole^2 sec)]. ——, present solution; – – –, Ames solution.

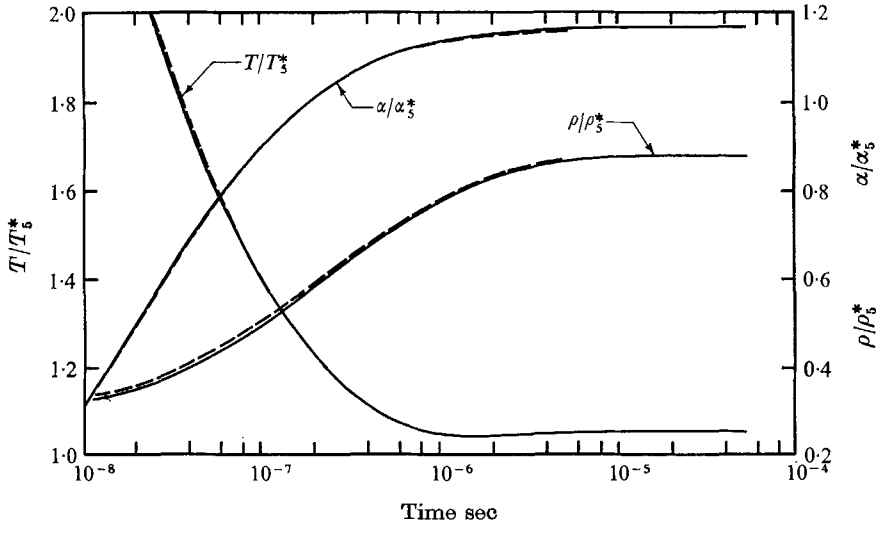

FIGURE 10. Comparison of solutions for end-wall thermodynamic properties in chemically relaxing O_2: $V_s = 3{\cdot}96$ km/sec, $T_1 = 294$ °K, $P_1 = 2$ torr and $k_r = 7{\cdot}3 \times 10^{21} T^{-2}$ [cm^6/(mole^2 sec)]. ——, present solution; – – –, Ames solution.

example, in figure 9 the variables T and α reach near-equilibrium values in about 10^{-6} seconds, while the variable ρ requires about 10^{-4} seconds. The reason for this behaviour is fairly obvious in view of the previous discussion in § 2. The temperature and the atomic-species mass fraction undergo rapid changes at first in order to establish a new state of chemical equilibrium, while the density continues to change, even after local equilibrium has been reached, owing to the continuing rise in the pressure level. The first effect, namely the change in T and α, occurs in a time of the order of the relaxation time in region 5, while the latter effect, the continued increase in density and pressure, is associated with the relaxation time in region 2. The values of T and α do not change significantly after a state of near equilibrium is attained because of the enormous energy required to further dissociate the gas, and the effect of relaxation in region 2 produces comparatively small changes in the energy level of the gas in region 5.

The time scales exhibited by these results depend directly on the magnitude of the reaction rate chosen. If the temperature dependence of the dissociation rate remains fixed, for example, while the magnitude of the rate is doubled, each point along the end-wall history would be reached in half the time. For the purpose of justifying this comment, at least for large values of time, consider the incident-shock region alone. Since all the properties at any one position in the relaxation zone, except distance from the shock wave, are coupled through the rate-independent conservation equations, doubling the reaction rate at all temperatures simply shortens the relaxation profiles by exactly a factor of two (Hanson & Watson 1966). Since the end-wall time scale is directly coupled to the scale of the incident-shock relaxation zone, all end-wall variations would also be shifted in time by a factor of two.

The effect of the rate magnitude for small values of time is more obvious. Doubling the reaction rate clearly doubles the rate-of-change of the wall pressure (as shown, for example, by the inner solution) and the atomic-species mass fraction. Since the rate-of-change of enthalpy is linearly coupled to the rate-of-change of pressure, only half as much time would be needed to reach the same values of P, h, α and T as before.

A second important observation which can be made from figures 9 and 10 is that the final values of T, α and ρ at the wall are quite different from the reference equilibrium values, and the deviations are noticeably larger for the stronger shock wave. The steady-state temperature and atomic-species mass fraction are both greater than their reference equilibrium values, while the density always remains below its reference equilibrium value. The explanation for these effects is simple enough. The element of gas immediately adjacent to the wall undergoes an entirely different history from those gas elements which are situated far from the wall (i.e. external to the entropy layer) and are processed to the reference equilibrium state. The important differences in the particle histories appear in the energy of the particles immediately after passage through the reflected shock wave, and in the amount of work which is done on the gas thereafter. For example, it is easy to show that additional energy is added to the gas near the wall because this gas is compressed from an initial state of lower density. The additional internal energy results in larger values for the temperature and atomic-species

mass fraction, and to be consistent with the thermal equation of state the final density is correspondingly decreased.

The magnitudes of these deviations are plotted as a function of shock strength in figure 11. Results are presented for the temperature, density and internal energy of chemically relaxing O_2. A superscript prime has been used to denote the steady-state value of a property evaluated at the wall. These results are only weakly dependent on the reaction rate employed in the calculations since the entropy-layer effect derives primarily from variations in the energy of the gas particles and not from the rate at which the particles adjust to their changing environment. The magnitudes of the entropy-layer deviations are clearly large enough to be significant for some shock-tube experiments.

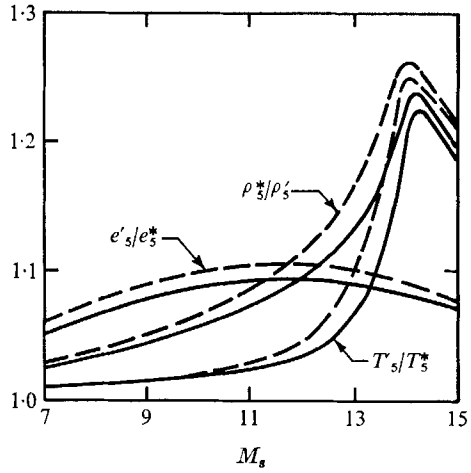

FIGURE 11. Final end-wall states in chemically relaxing O_2: $T_1 = 297\,°\text{K}$. P_1: – –, 1 torr; ——, 5 torr.

The results presented in figure 11 represent the maximum degree of thermodynamic non-uniformity within the entropy layer since the deviations are largest at the wall. Another important parameter is the spatial extent of the layer. If one defines a relaxation length behind the incident shock wave, L_2, then the entropy-layer thickness in region 5 is (by simple geometry) given approximately by

$$L_5 \simeq L_2 V_r/(V_r + V_s). \tag{40}$$

The proper value for the reflected-shock speed in this case is the final equilibrium value. Typical values for the entropy-layer thickness in O_2 are shown in figure 12 for two different initial pressures. Also plotted is the entropy-layer formation time, taken here to be simply the laboratory value for the relaxation time in region 2, i.e.

$$\tau_{2L} = L_2/V_s. \tag{41}$$

For these cases of chemical relaxation, the relaxation length in the incident-shock flow has been defined to be the distance at which the atomic-species mass

fraction reaches 90 % of its equilibrium value. The results presented of course depend strongly on the dissociation rates employed, namely

$$k_{d,O_2} = 2{\cdot}25 \times 10^{12} T^{\frac{1}{2}} (\theta_d/T)^{1{\cdot}5} \exp(-\theta_d/T) \tag{42}$$

and

$$k_{d,O} = 2{\cdot}8 k_{d,O_2} \tag{43}$$

(Wray 1962). Different rates are used for atomic and molecular collision partners in order to account for the recognized increase in the efficiency of the atomic

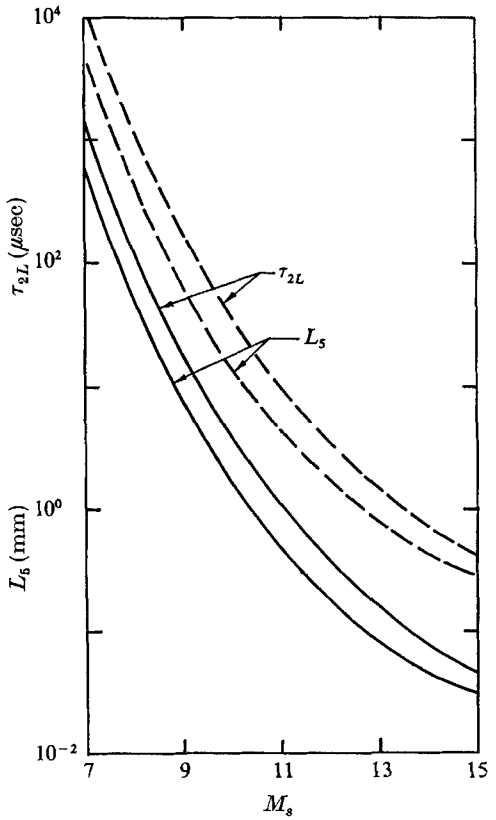

FIGURE 12. Entropy-layer thickness (L_5) and entropy-layer formation time (τ_{2L}) in chemically relaxing O_2: $T_1 = 297$ °K, $k_{d,O_2} = 2{\cdot}25 \times 10^{12} T^{\frac{1}{2}} (\theta_d/T)^{1{\cdot}5} \exp(-\theta_d/T)$ and $k_{d,O} = 2{\cdot}8 k_{d,O_2}$ [cm³/(mole sec)]. P_1: – –, 1 torr; ——, 5 torr.

species in promoting dissociation. According to figure 12, the entropy-layer thickness becomes greater than 1 mm for shock strengths less than about Mach 12 if the initial pressure is 1 torr, and shock strengths less than about Mach 10 if the initial pressure is 5 torr.

It is worth remembering at this point that the effect of heat transfer to the end-wall has not been considered in the present discussion, and this phenomenon would act in a real situation to modify the entropy layer induced by relaxation processes.

We turn our attention now to vibrational relaxation. For a vibrationally relaxing gas the calculation of the time-varying thermodynamic properties is some-

what simpler. The energy equation, (28), remains the same, but the appropriate caloric equation of state for a diatomic (or linear triatomic) molecule is simply

$$h = \tfrac{7}{2}RT + \sigma. \tag{44}$$

Again the pressure solution and the initial end-wall state are presumed known from the outer and inner solutions. The solution for the thermodynamic state proceeds by simultaneously integrating (28) and the rate equation, (13), so that at each step in time we can find, in turn, new values of h, σ, T and τ. The thermal equation of state,

$$P = \rho RT, \tag{45}$$

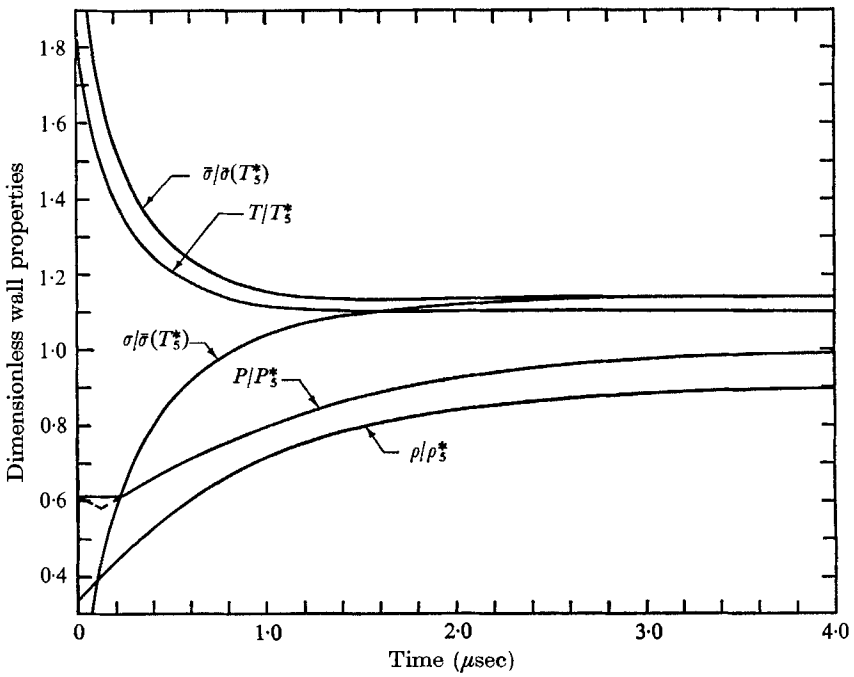

FIGURE 13. Solution for end-wall thermodynamic properties in vibrationally relaxing CO_2: $V_s = 1{\cdot}62$ km/sec, $T_1 = 300$ °K and $P_1 = 1$ torr. Johannesen *et al.* (1967) relaxation rate.

is needed only to calculate the density, if that quantity is desired. For vibrational relaxation the calculations are actually simple enough that they may be carried out with reasonable speed and precision by hand.

Figure 13 provides the computed results for the case of shock-wave reflexion in CO_2 for which the outer and inner solution were presented earlier (see figures 4 and 8). Unfortunately a characteristics solution is not available for quantitative comparison, but the character of the results is in agreement with the solution presented by Johannesen *et al.* (1967) for their 'universal' diatomic gas. Thermodynamic histories were computed using both of the inner solutions presented in figure 8, but the differences were for the most part too small to be distinguished on this figure. (The results shown were computed with the constant-pressure inner solution.)

The presence of two separate time scales in the wall properties is less marked

for vibrational relaxation, thus permitting the results to be plotted with a linear time scale. The time required for the temperature to approach within a few per cent of its steady-state value is less than 1 μsec, while the pressure and density both require about 4 μsec to attain this same deviation from their final values. The ratio of these times is about what one would expect from the consideration of relaxation-time ratios presented in § 2 of this paper. The separation of the two time scales for the pressure history is much greater, however, because of

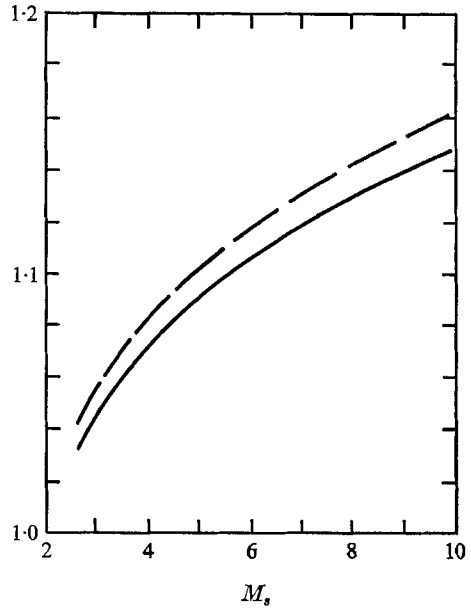

FIGURE 14. Final end-wall properties in vibrationally relaxing CO_2: $T_1 = 300$ °K and $\gamma_1 = 1{\cdot}4$. ——, $T_5'/T_5^* = \rho_5^*/\rho_5'$; – – –, e_5'/e_5^*.

the relative influence of the relaxation in regions 2 and 5, also discussed earlier. It is this increased separation in the time scales of the pressure history which makes the outer solution so successful, and it is this success which permits one to calculate simply and accurately the wall histories of the remaining thermodynamic variables.

The steady-state deviations from the reference equilibrium state are qualitatively the same for a vibrationally relaxing gas as exhibited earlier by a chemically relaxing gas; i.e. the final temperature and internal energy at the wall are larger and the density is smaller than the reference equilibrium values. These are the results to be expected for all forms of relaxation. The magnitudes of these deviations in CO_2 are plotted for a range of shock speeds in figure 14. Again the results depend very little on the actual relaxation rates employed.

The spatial extent and the formation time of relaxation entropy layers in CO_2 are shown in figure 15. The definition of L_5 is the same as (40) while L_2 and τ_{2L} are based simply on the frozen conditions in region 2, i.e.

$$P_1 L_2 = (P_1 \tau_{2L}) V_s \tag{46}$$

and

$$P_1 \tau_{2L} = P_1 (P\tau)_{2F} / (\eta P_2)_{2F}. \tag{47}$$

The relaxation rate employed is the one specified in (14). The thickness of the entropy layer is seen to be greater than 1 mm for shock waves of strength less than Mach 4·6 and an initial pressure of 1 torr.

The thicknesses predicted by figure 15 are in reasonable agreement with Johannesen's experimental observations (see, for example, figure 8 of Johannesen *et al.* 1967), but the magnitude of the density decrement predicted by figure 14 is greater than the value actually measured owing to our neglect of heat-transfer effects.

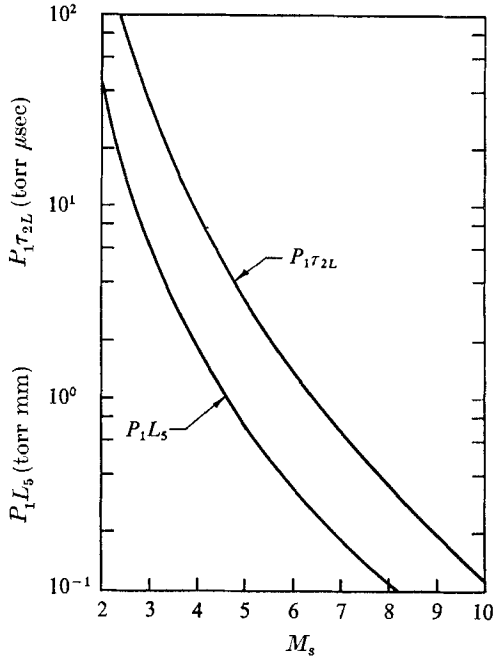

FIGURE 15. Entropy-layer thickness (L_5) and entropy-layer formation time (τ_{2L}) in vibrationally relaxing CO_2: $T_1 = 300$ °K and $\gamma_1 = 1{\cdot}4$. Johannesen *et al.* (1967) relaxation rate.

5. Conclusions

The problem of shock-wave reflexion in a relaxing gas has been investigated. It was shown that the wall pressure is characterized by two different time scales. The separation in these time scales allows formulation of simple inner and outer solutions for the pressure history which are in good agreement with numerical calculations based on the method of characteristics. Since the overall pressure behaviour is strongly dominated by the relaxation behind the incident shock wave, the outer solution provides a good fit to the exact pressure history for all but very short times after reflexion. The simplicity of the outer solution, essentially a direct mapping of the spatial distribution of density behind the incident shock wave into a temporal distribution of pressure on the wall, should make the model particularly useful for rate-measurement studies.

Knowledge of the pressure solution enables computation of the time evolution of other thermodynamic variables in the gas adjacent to the wall. Results based

on this model are in excellent agreement with those computed using the method of characteristics, although the simple model requires only a small fraction of the computing time.

An interesting result of the non-steady reflexion process is the formation of a non-uniform entropy layer adjacent to the end-wall. Numerical results have been presented to describe the non-uniformity and spatial extent of this layer in chemically relaxing O_2 and vibrationally relaxing CO_2. These results are pertinent to investigations which depend on shock-wave reflexion as a means of obtaining a well-defined sample of uniform high-temperature gas.

For additional results and discussion of this problem, see Hanson (1968).

The author wishes to express his appreciation to Prof. D. Baganoff of Stanford University and Mr L. Presley of Ames Research Center for their willingness to discuss problems which arose in this work. Thanks also go to Mrs Elsie Williams of Ames Research Center for her invaluable assistance with the computer programming.

This research was conducted while the author held a NASA Traineeship in the Department of Aeronautics and Astronautics at Stanford University. Portions of the work were supported by the National Aeronautics and Space Administration under grant NGR 05-020-245.

Appendix. Reaction-rate relation behind the incident shock wave

Using a co-ordinate system fixed to the incident shock wave (region 1 upstream and region 2 downstream), one can write, for the downstream pressure,

$$P_2 = P_1 + \rho_1 V_s^2(1 - 1/\eta) \simeq \rho_1 V_s^2(1 - 1/\eta). \tag{A 1}$$

Changes in pressure owing to changes in density are therefore specified by

$$dP_2 = \rho_1 V_s^2 d\eta/\eta^2, \tag{A 2}$$

or, in dimensionless form,

$$dP_2/P_2 \simeq (d\eta/\eta)/(\eta - 1). \tag{A 3}$$

The subscript 2 will hereafter be taken as understood.

Since the flow is assumed to be adiabatic, differential changes in pressure between adjacent flow-field points are also given by

$$dP = \rho\, dh. \tag{A 4}$$

Dividing (A 4) by the thermal equation of state, (31), we obtain

$$dP/P = dh/[RT(1 + \alpha)]. \tag{A 5}$$

If we restrict our attention to the conditions immediately behind the shock front, then $\alpha \equiv 0$ and the differential form of the caloric equation of state (see (29)) is simply

$$dh = [\tfrac{3}{2}RT + D - \bar{\sigma}]\, d\alpha + \tfrac{7}{2}R\, dT + d\bar{\sigma}. \tag{A 6}$$

For the temperatures of interest here (i.e. $T_2 > \theta_v$)

$$d\bar{\sigma} = (\partial\bar{\sigma}/\partial T)\, dT \simeq R\, dT \tag{A 7}$$

so that (A 5) can be rewritten as

$$dP/P \simeq [\tfrac{3}{2}+\theta_d/T-\bar{\sigma}/RT]\,d\alpha+\tfrac{9}{2}\,dT/T. \tag{A 8}$$

Solving for dT/T we obtain

$$dT/T \simeq \tfrac{2}{9}[dP/P-(\tfrac{3}{2}+\theta_d/T-\bar{\sigma}/RT)\,d\alpha]. \tag{A 9}$$

Using the differential form of the thermal equation of state,

$$dP/P = d\rho/\rho+dT/T+d\alpha/(1+\alpha) = d\eta/\eta+dT/T+d\alpha, \tag{A 10}$$

and substituting (A 9) and (A 3) to eliminate dT/T and dP/P respectively, one can finally write $d\eta$ in terms of $d\alpha$,

$$d\eta \simeq \tfrac{2}{9}\eta[1-\tfrac{7}{9}(\eta-1)^{-1}]^{-1}\Psi(T)\,d\alpha, \tag{A 11}$$

where

$$\Psi(T) = (\theta_d/T-3-\bar{\sigma}/RT).$$

A more useful form of (A 11) is simply

$$D\eta/Dt \simeq \tfrac{2}{9}\eta[1-\tfrac{7}{9}(\eta-1)^{-1}]^{-1}\Psi(T)\,(D\alpha/Dt). \tag{A 12}$$

REFERENCES

Baganoff, D. 1965 *J. Fluid Mech.* **23**, 209.

Hanson, R. K. 1968 Ph.D. thesis, Stanford University; also *Stanford Univ. SUDAAR* no. 345.

Hanson, R. K. 1970 (To be published.)

Hanson, R. K. & Watson, R. 1966 *A.I.A.A. J.* **4**, 749.

Johannesen, N. H., Bird, G. A. & Zienkiewicz, H. K. 1967 *J. Fluid Mech.* **30**, 51.

Johannesen, N. H., Zienkiewicz, H. K., Blythe, P. A. & Gerrard, J. H. 1962 *J. Fluid Mech.* **13**, 213.

Millikan, R. C. & White, D. R. 1963*a* *J. Chem. Phys.* **39**, 3209.

Millikan, R. C. & White, D. R. 1963*b* *J. Chem. Phys.* **39**, 98.

Presley, L. L. & Hanson, R. K. 1969 *A.I.A.A. J.* **7**, 2267; also *A.I.A.A. preprint* no. 68–732.

Vincenti, W. G. & Kruger, C. H. 1965 *Introduction to Physical Gas Dynamics.* Wiley.

Wray, K. L. 1962 In *Hypersonic Flow Research* (ed. F. R. Riddell), p. 187. Academic.